Phase diagram of nitrous oxide: Analogy with carbon dioxide

V. Iota, J-H. Park, and C. S. Yoo
Lawrence Livermore National Laboratory, Livermore, California 94551, USA
(Received 10 September 2003; published 18 February 2004)

We present the phase diagram for nitrous oxide (N_2O) derived from *in situ* high pressure and temperature Raman and x-ray diffraction studies. Two new phases (II and IV) are discovered above 600 K between 18 and 50 GPa; both are quenchable to ambient temperature. The crystal structures and stability fields of N_2O phases are similar to those of CO_2 below 50 GPa and 800 K. However, we found subtle differences in their physical properties and crystal structures, indicating an increased disparity (or ionicity) between N—N and N—O bonds in bent N_2O-IV (*Pbcn*). The present results thus explain the divergence observed at higher pressures and temperatures; N_2O disproportionates into ionic $NO^+NO_3^-$ and N_2, whereas CO_2 polymerizes into an extended covalent solid.

DOI: 10.1103/PhysRevB.69.064106 PACS number(s): 64.70.Kb, 62.50.+p, 71.15.Nc, 81.05.−t

INTRODUCTION

The phase stability of simple molecular solids is generally predicated on a well-defined separation in energy scale between strong intramolecular interactions, and relatively weak intermolecular bonds. At higher densities, however, this energy separation begins to break down, as rapid gains in electron kinetic energy result in increased repulsive intermolecular interactions. This results in structural phase transitions to configurations with softer potentials and more delocalized electrons. Electron delocalization can occur along different paths, leading to nonmolecular phases: covalently bonded polymers in N_2 and CO_2,[1,2] a charge transferred solid in H_2,[3] metallic phases in O_2,[4] or an ionic solid in N_2O.[5,6]

While pressure-induced electron delocalization explains qualitatively the molecular-to-nonmolecular phase transition, recent studies[7,8] show that, because of the existence of intermediate phases, metastability, kinetics, and lattice strain, the detailed mechanisms of delocalization are substantially complex. The phase diagram of CO_2, as reproduced in Fig. 1,[7] is a good example showing such complexity. For example, *in situ* high pressure and temperature experiments[7] of CO_2 show that molecular phase I ($Pa3$) is only stable within a limited range of pressures (<11 GPa) and temperatures (<500 K) and that, at higher pressures and temperatures, it transforms into molecular configurations with more itinerant electrons: first to pseudo-sixfold-coordinated phase II ($P4_2/mnm$ or *Pnnm*) and bent phase IV (*Pbcn* or $P4_12_12$), both with elongated molecular bonds and compressed intermolecular distances, and finally to a fully extended phase V ($P2_12_12_1$), made of fourfold-coordinated carbon atoms. These experimental results suggest that the electron delocalization occurs gradually, via intermediate phases (II, IV, and III to an extent) to a fully extended covalent solid (V). The formation of intermediary phases lowers the barrier to breaking the strong C═O molecular double bonds to form singly bonded tetrahedral CO_4 structures.

Recent total energy calculations of CO_2, however, paint a different picture, asserting that the high pressure, ''intermediate'' phases may be strictly molecular and have entirely different phase stabilities as reproduced in Fig. 1 in red.[9] This calculation fails to account for the stability of the bent phase IV (*Pbcn*) and, instead, suggests that a molecular *Cmca* structure occupies the entire stability field of phase IV.[7] This description advocates an extended stability domain for molecular CO_2 and seems to imply that the molecular-to-nonmolecular transition occurs abruptly at the interface between phases III and V.

The phase diagram of nitrous oxide (N_2O) offers the ideal template to resolve this disagreement; CO_2 and N_2O are isoelectronic, linear triatomics with similar molecular weights, melting temperatures, and quadrupole moments. Although N_2O has no inversion symmetry, it has been shown to resonate between two bonding configurations with opposing dipole moments: $^-N{=}N^+{=}O$ and $N{=}N^+{=}O^-$.[10] As a result, the net dipole moment of nitrous oxide is negligible compared to its substantial quadrupole moment.[11,12] In the absence of dipole ordering, N_2O molecules are oriented randomly and crystallize in the same configurations as CO_2,[13] as phase I ($Pa3$) at 1 GPa and phase III (*Cmca*) above ~5

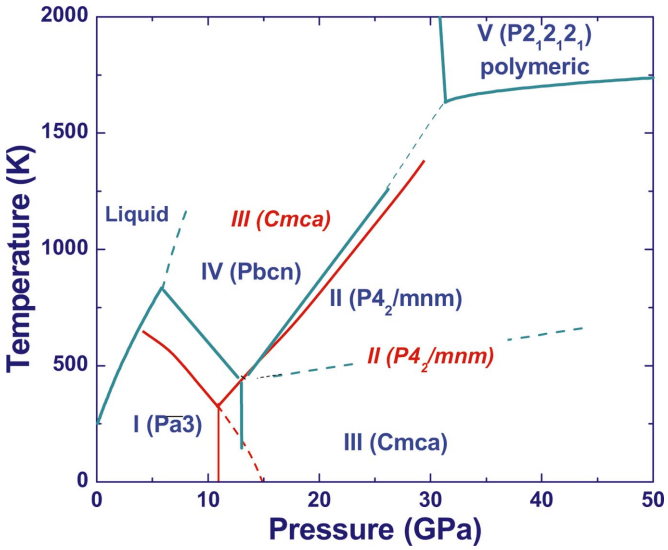

FIG. 1. (Color) Phase diagram of CO_2 as previously determined in the experiments in black (reproduced from Ref. 7) and theoretical calculations in red (from Ref. 9).

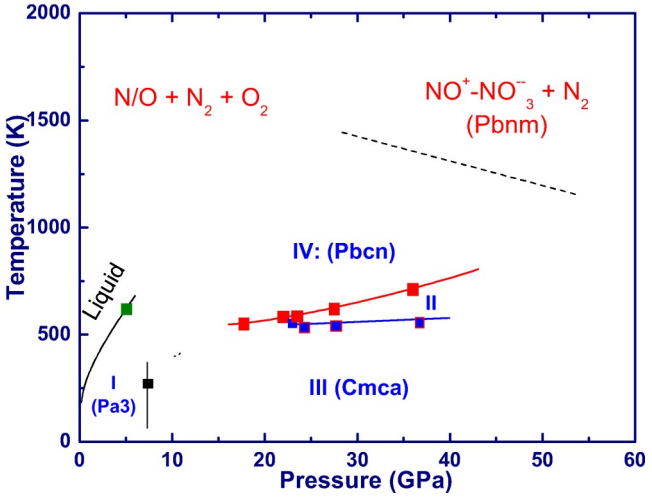

FIG. 2. (Color online) Phase transformation diagram of N_2O. Each data point represents a pressure-temperature coordinate where the phase transformation was observed. The phase boundaries were constructed by connecting these data points. The chemical changes of N_2O above the dotted line are based on the work previously reported in Ref. 6.

GPa. However, the one-to-one phase analogy between CO_2 and N_2O breaks down dramatically at higher pressures and temperatures. Above 35 GPa and 1000 K, CO_2 forms an extended network solid based on CO_4 tetrahedra,[7] whereas N_2O disproportionates to form an ionic solid $NO^+NO_3^-$ and N_2.[5,6]

In this paper, we report the discovery of two new phases of N_2O (labeled II and IV in analogy with CO_2) and compare their properties with those of the corresponding CO_2 phases; we find subtle differences in properties and crystal structure accounting for the diverging delocalization paths for the two isoelectronic molecules.

EXPERIMENTAL METHODS

Liquid nitrous oxide samples were loaded cryogenically into diamond anvil cells (DACs) by compressing 99.99% pure N_2O gas to 10 bars at 233 K in a home-built autoclave. The loading vessel was purged with dry N_2O gas prior to loading, in order to avoid sample contamination. For *in situ* heating experiments, we used electric coil heaters wrapped around the DAC to achieve temperatures typically up to 750 K. The temperature of the sample was continuously monitored during experiments by using a *K*-type thermocouple in contact with one of the anvils. We estimate the error in temperature to be less than 10 K. Pressure was determined using the R_1 luminescence line from micrometer-sized ruby ($Al_2O_3:Cr^{2+}$) chips placed in the sample and the standard high temperature-pressure calibration curve.[14] Since the ruby luminescence broadens significantly at high temperatures, we estimate the error in pressure to be up to 10% at 750 K.

The samples were monitored visually during experiments using a microscope equipped with a charge-coupled device (CCD) camera. Raman spectra were measured using the 514.5 nm line of an Ar^+ laser and a SPEX triple grating monochromator equipped with a CCD detector. Angle-resolved powder x-ray diffraction data of N_2O phases were obtained by using focused monochromatic x ray from the High Pressure Collaborating Access Team (HPCAT) beamline at the Advanced Photon Source (APS, $\lambda = 0.3738$ Å)

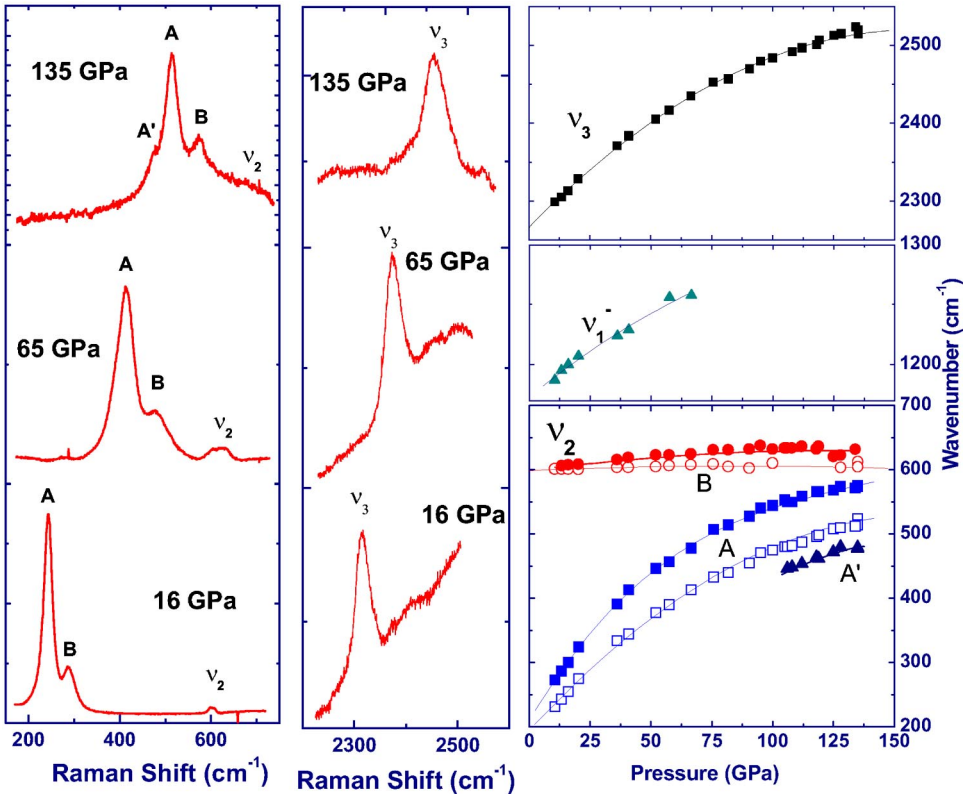

FIG. 3. (Color online) Raman spectra of N_2O-III at high pressures. Note that N_2O-III shows relatively sharp Raman features and remains transparent even at 135 GPa. The separation between the external and internal modes is apparent to well above 100 GPa, indicating a strong molecular nature of N_2O-III. This behavior of N_2O-III is in contrast to that of CO_2-III. The ν_1' band emerges into the strong diamond Raman band above 70 GPa.

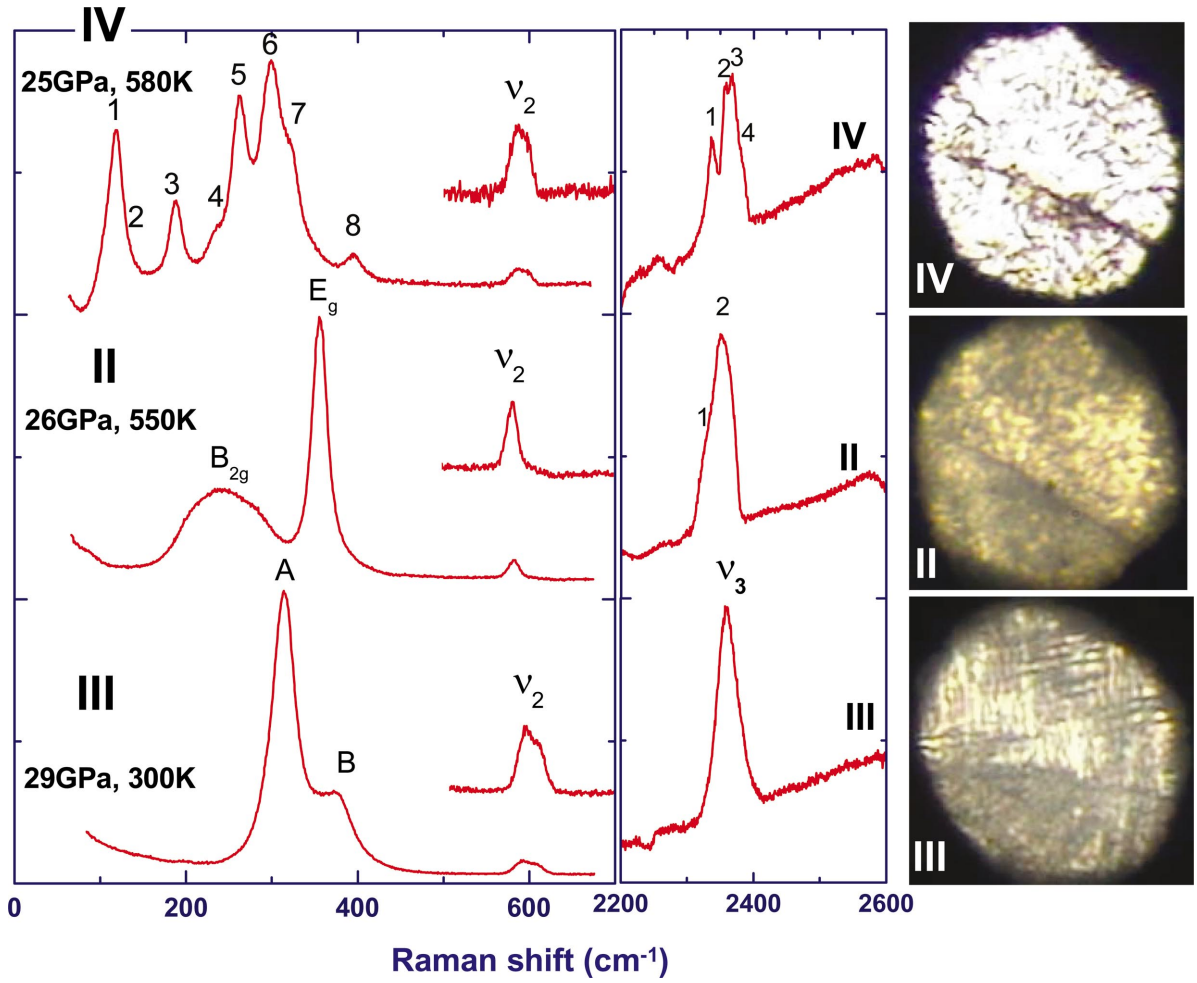

FIG. 4. (Color) Raman spectra and microphotographs of high pressure and temperature phases of N_2O, measured in a heated DAC. The one-to-one correlation with the CO_2 phases (Ref. 7) is apparent especially in the external lattice modes, suggesting largely similar configurations for the corresponding phases.

and Stanford Synchrotron Radiation Laboratory (SSRL, $\lambda = 0.6199$ Å). A series of Debye-Sherrer diffraction rings were recorded between $2\theta = 5°$ and 35° on high-resolution image plates (MAR345 at the HPCAT and Fuji BAS2500 at the SSRL). The FIT2D program[15] was then employed to convert the two-dimensional (2D) image-plate records into 1D data for structural refinement by using the General Structure Analysis System.[16]

RESULTS AND DISCUSSION

Figure 2 summarizes the results of the present experiments in the form of a phase transformation diagram. The Raman spectra of phases I and III were previously described to 40 GPa at ambient temperature.[17] In the present study, we extended those studies to 135 GPa and found that phase III remains stable in this entire pressure range at 300 K as illustrated in Fig. 3. The sample also appears to be transparent even at 135 GPa. Note that the external lattice modes are well separated from the internal vibration modes to well above 100 GPa, and no softening of modes is apparent to 135 GPa, the maximum pressure applied in this study. Clearly, it indicates a strong molecular nature of N_2O-III. In contrast, we reported that the Raman spectrum of CO_2-III is smeared considerably with pressure and becomes completely washed out above ~80 GPa.[7] This was attributed to an unusually large lattice strain in CO_2-III, evident from its high bulk modulus (~80 GPa) and large pressure gradient within samples (~100 GPa/mm at 50 GPa).[7] Note that the broadening of Raman lines in N_2O is substantially less pronounced even at 135 GPa (Fig. 3), suggesting that N_2O-III supports a considerably smaller amount of lattice strain than CO_2-III. This result is also consistent with a relatively soft bulk modulus of N_2O-III (11–20 GPa).[6]

Above ~600 K, we observe two new N_2O phase (labeled II and IV in Fig. 2). Phase II stabilizes above 23 GPa in a relatively narrow temperature range of 10–30 K. Phase IV, on the other hand, is obtained by heating either phase III below 23 GPa, or phase II at higher pressures. These transformations can be readily observed by abrupt changes in the visual appearance of the sample and in the Raman spectrum (Fig. 4). Note that, because of the absence of inversion symmetry in N_2O, the bending (ν_2) and asymmetric stretching (ν_3) internal modes are always Raman active. However, we find that the relative intensity of ν_2 continuously increases in

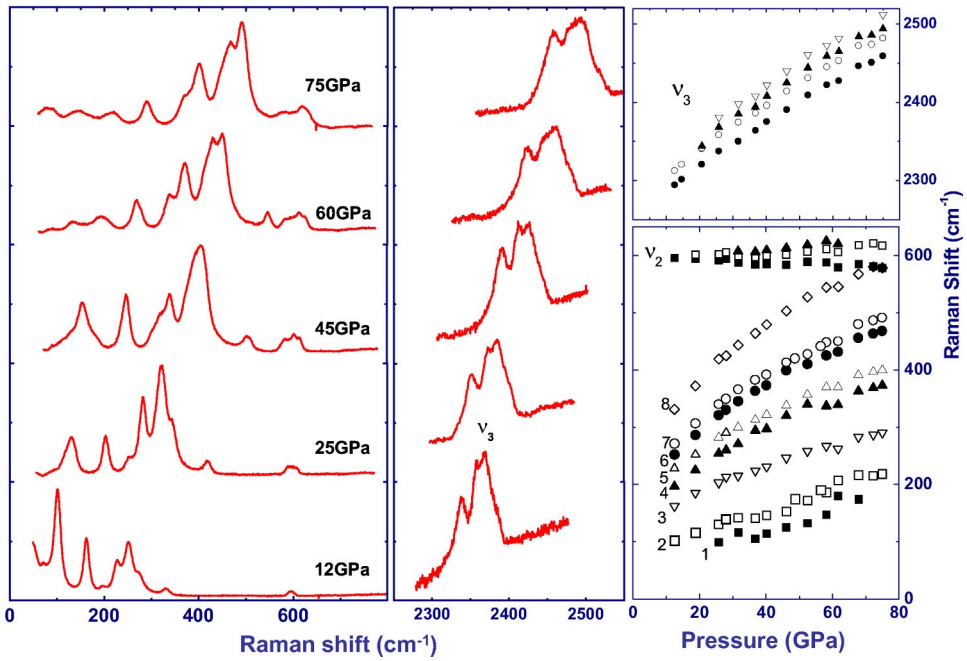

FIG. 5. (Color online) Raman spectra of quenched N_2O-IV at high pressures, showing relatively sharp Raman features to 75 GPa. This is in contrast to CO_2-IV, whose Raman spectra are entirely smeared out above 70 GPa. The ν_3 asymmetric internal mode is split into four components in phase IV, indicating a lower symmetry crystal structure consistent with four bent N_2O molecules in a primitive unit cell found in x-ray studies (see Fig. 6).

N_2O-IV with increasing pressures. We attribute the intensity enhancement in ν_2 to the bending of N_2O molecules (similar to the bending observed in CO_2-IV), also evident from the x-ray data which will be shown later in Figs. 6 and 7.

Both high temperature phases II and IV are quenchable to room temperature even under relatively slow cooling over several hours. At 300 K, both quenched phases remain stable on decompression down to ~5 GPa where they transform back to N_2O-I. Upon compression, the quenched phase IV shows high stability well above 100 GPa, bypassing the entire stability field of phase III. The quenched phase IV also retains its relatively sharp Raman characteristic spectrum remarkably well even at 75 GPa (shown in Fig. 5), noting another apparent difference from CO_2. The Raman spectrum of quenched CO_2-IV, for example, completely disappears above 70 GPa, indicating the transformation to a covalently bonded amorphous solid.[7] These differences in phases IV and the above-mentioned III clearly indicate that, upon compression, CO_2 molecules develop substantially stronger intermolecular bonds (or more pronounced electron delocalization) than N_2O.

Note in Fig. 2 that N_2O-II can be obtained only by heating phase III above 20 GPa, similarly to CO_2-II in Fig. 1. However, the stability field of N_2O-II is substantially narrower in temperature than that of CO_2-II. This permits N_2O-II to transform directly into N_2O-IV between 6 and 20 GPa. This, again, is different from CO_2, for which phase III is likely metastable and its direct transformation to phase IV is forbidden kinetically.[7,9] Nevertheless, a relatively small temperature dependence of the III to II phase boundary still points to the presence of a large kinetic barrier and thus to a large disparity between the inter- and intramolecular bonding of phases III and II.

The crystal structures of phase III and IV, as determined from angle-resolved x-ray diffraction, also indicate sharp differences in intermolecular interaction and chemical bonding between the two phases. Because of the relatively narrow pressure-temperature stability field of N_2O-II, we were unable to obtain a high quality, single-phase diffraction pattern of this polymorph. High quality diffraction patterns, however, were obtained from N_2O-III and IV (Fig. 6). The patterns appear to be similar to those of the corresponding CO_2 phases, with subtle—but notable—differences. The diffraction pattern of N_2O-III at 5 GPa and ambient temperature can be interpreted in terms of an orthorhombic *Cmca* unit cell with $a=4.987(1)$ Å, $b=4.533(1)$ Å, and $c=6.220(1)$ Å with a few exceptions: two peaks (010) and (110) violating a *c* center and a peak (102) violating a glide along the *c* axis. The limited number of reflections observed, however, preclude any further refinement for any primitive cell with four orientation-ordered molecules. In this *Cmca*

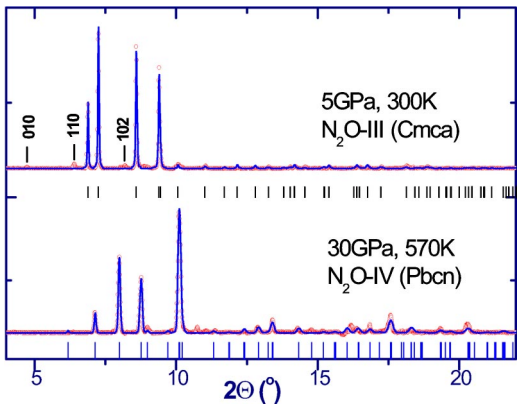

FIG. 6. (Color online) X-ray diffraction patterns of (a) N_2O-III (*Cmca*) at 5 GPa and 300 K and (b) N_2O-IV (*Pbcn*) at 30 GPa and 570 K, after removing featureless backgrounds. The experimental data are indicated in symbols, the Rietveld refined results in lines, and the *hkl* reflections in vertical bars. Corresponding *R* factors are $R_{wp}=0.0300$, $R(F^2)=0.2776$ for N_2O-III and $R_{wp}=0.01$ and $R(F^2)=0.2724$ for N_2O-IV.

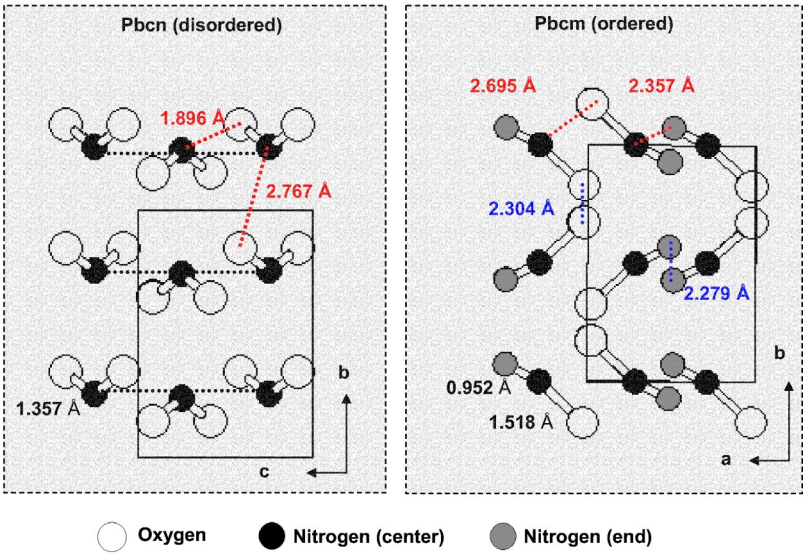

FIG. 7. (Color online) Crystal structures of (a) disordered N_2O-IV (*Pbcn*) and (b) ordered N_2O-IV (*Pbcm*) at 30 GPa and 570 K. In both models, the N_2O molecules are bent and the center N atoms occupy the fcc sites. The ordered structure displays a significant disparity between N—N and N—O bond lengths; this increased ionicity in phase IV facilitates the ionic disproportionation of N_2O previously observed at higher pressures and temperatures (Refs. 5 and 6).

structure, the center N atom is at the origin and the end N and O atoms are at (0 0.2811(4) 0.3975(3)), respectively. N_2O molecules remain linear with an average N═O and N═N distance of 1.179(2) Å and a nearest N(center)···O(N) intermolecular distance of 2.842(2) Å. Note that the intermolecular distance is about 2.4 times the intramolecular distance, a substantially greater disparity than that of CO_2-III (~2.0 times). This result, again, indicates a stronger molecular character for N_2O-III compared to CO_2-III.

The systematic absence of peaks in the diffraction pattern of N_2O-IV at 30 GPa and 570 K (Fig. 6) is consistent with an orthorhombic *Pbcn* unit cell with $a=4.2356(6)$ Å, $b=5.9825(10)$ Å, and $c=4.2232(13)$ Å. The best diffraction profile refinement yields the center N at (0 0.256(1) 0.25) and the end site N/O at (0.243(1) 0.349(1) 0.415(1)). In this orientation-disordered model [Fig. 7(a)], the average intramolecular bond distance is 1.360(4), substantially elongated from that of N_2O-III, and the intermolecular distance is 1.891(5) Å, substantially shorter than that of N_2O-III. Similarly to CO_2-IV, N_2O molecules are bent with N—N—O angle of 131.8(9)°.

The crystal structure of N_2O-IV shows an important difference from that of CO_2-IV. That is, the center nitrogen atoms in N_2O-IV occupy the face-centered-cubic (fcc) sites [Fig. 7(a)]; whereas the carbon atoms in CO_2-IV deviate from the fcc packing and form zigzag chains. This difference results in a perfect layer structure and a relatively large bending angle 132° in N_2O, but in a large buckling of CO_2 layers and a substantially smaller bending angle 170° in CO_2. We consider the reason for the divergence to be due to the difference in ionicity (or covalency) between N_2O and CO_2. To examine this hypothesis, we have refined the x-ray diffraction pattern of N_2O-IV based on an ordered model. Although not unique,[18] a reasonable solution was found in *Pbcm* with $a=4.231(2)$ Å, $b=5.987(2)$ Å, and $c=4.237(1)$ Å. This ordered crystal structure exhibits a large disparity between N—N [0.9615(3) Å] and N—O [1.5120(5) Å] bonds [see Fig. 7(b)] and, thus, suggests a relatively high level of ionicity in N_2O-IV. This N—N distance represents nearly that of N≡N triple bonds and the N—O distance is close to that of single bonds. Note that the average distance of N—N and N—O is approximately same as that of the *Pbcn* mentioned above. Furthermore, in this model the nearest neighbor of the center N is the end N at 2.3566(3) Å and the end N to the next neighboring end N distance is 2.2787(3) Å, revealing a channel for the disproportionation of N_2O molecules into NO—NO_3 and N_2 as previously observed.[5,6]

SUMMARY

The phase transformation diagrams in Figs. 1 and 2 allows us to compare the stabilities and properties of CO_2 and N_2O phases over a wide range of pressures and temperatures. Although the phase diagram of N_2O is similar to that of CO_2, with isostructural polymorphs, the present study reveals several important differences. (1) N_2O-III is more molecular in nature than CO_2-III. (2) N_2O-IV is more ionic than CO_2-IV. (3) N_2O ionizes whereas CO_2 polymerizes. The close phase parallelism is maintained mainly in a molecular regime where electrons are localized within intramolecular bonds and quadrupole interactions are dominant. Upon breaking or weakening of N═O (C═O) bonds, the different nature of carbon and nitrogen enhances the ionic character in N_2O phases and eventually leads to ionization of N_2O either to $NO^+NO_3^-$ and N_2 or to dissociation to N_2 and O_2. In contrast, in CO_2-IV, higher covalency and stiffer intermolecular bonds lead to the formation of a fully extended covalent solid, CO_2-V.

While the existence and stability of bent CO_2-IV and N_2O-IV are apparent in the present and previous experiments,[7] theoretical descriptions of such phases face challenges.[9] Considering that transformation kinetics plays an important role in determining the phase stability of both N_2O and CO_2 (and very likely other molecular compounds), any calculation aiming to predict their phase stabilities *must* include molecular dynamics simulations of a large number of structural configurations and reaction paths in addition to the minimum energy calculations.

ACKNOWLEDGMENTS

We thank Dr. Baer, Dr. Cynn, Dr. Evans, Dr. Lipp, and Mr. Visbeck of the High Pressure Physics Group at the LLNL, for their experimental assistance. The x-ray experiments were done at the 16ID-B beamline of the HPCAT at the APS. The HPCAT is a collaboration among the Carnegie Institution, the Lawrence Livermore National Laboratory, the University of Hawaii, the University of Nevada–Las Vegas, and the Carnegie/DOE Alliance Center (CDAC). We thank the HPCAT staff, Dr. Somayazulu and Dr. Hausermann in particular, for their technical assistance. The work has been supported by the LDRD and PDRP programs at the LLNL, University of California under the auspices of the U.S. DOE under Contract No. W-7405-ENG-48.

[1] A. F. Goncharov, E. Gregoriantz, H. K. Mao, Z. Liu, and R. J. Hemley, Phys. Rev. Lett. **85**, 1262 (2000).
[2] V. Iota, C. S. Yoo, and H. Cynn, Science **283**, 1510 (1998).
[3] R. J. Hemley, Z. G. Soos, M. Hanfland, and H. K. Mao, Nature (London) **369**, 384 (1994).
[4] G. Weck, P. Loubeyre, and R. LeToullec, Phys. Rev. Lett. **88**, 035504 (2002).
[5] M. Somayazulu, A. Madduri, A. F. Goncharov, O. Tschauner, and P. F. McMillan, Phys. Rev. Lett. **87**, 135504 (2001).
[6] C. S. Yoo, V. Iota, H. Cynn, M. Nicol, T. Le Bihan, and M. Mezouar, J. Phys. Chem. **107**, 5922 (2003).
[7] Please see our previous studies V. Iota *et al.*, Phys. Rev. Lett. **83**, 5527 (1999); **86**, 5922 (2001); **86**, 444 (2001); Phys. Rev. B **65**, 104145 (2002); (to be published).
[8] M. L. Erements, R. J. Russell, H. K. Mao, and E. Gregoryanz, Nature (London) **411**, 170 (2001).
[9] S. Bonev, G. Galli, and F. Gygi, Phys. Rev. Lett. **91**, 065501 (2003).
[10] L. Pauling, *Nature of the Chemical Bond* (Cornell University Press, Ithaca, NY, 1940).
[11] B. Kuchta and R. D. Etters, J. Chem. Phys. **95**, 5399 (1991).
[12] D. E. Stogryn and A. P. Stogryn, Mol. Phys. **11**, 371 (1966).
[13] R. L. Mills, B. Olinger, D. T. Cromer, and R. LeSar, J. Chem. Phys. **95**, 5392 (1991).
[14] J. Yen and M. Nicol, J. Appl. Phys. **72**, 5535 (1992).
[15] A. P. Hemmersley, ESRF Report No. 98HA01T, 1998 (unpublished).
[16] A. C. Larson and R. B. von Dreele, Los Alamos National Laboratory Report No. LAUR 86-748, 1994 (unpublished).
[17] H. Olijnyk, H. Däufer, M. Rubly, H.-J. Jodl, and H. D. Hochheimer, J. Chem. Phys. **93**, 45 (1990).
[18] An equally good fit is obtained by using an ordered $P4_12_12$ structure. This alternate model shows only minor differences from the *Pbcm* and hence all subsequent discussions in the text hold.